◆ Human Brain Mapping 8:182–193(1999) ◆

Modeling Extended Sources of Event-related Potentials Using Anatomical and Physiological Constraints

Wilhelm Emil Kincses,[1] Christoph Braun,[1]* Stefan Kaiser,[1] and Thomas Elbert[2]

[1]*Institute of Medical Psychology, University of Tübingen, Germany*
[2]*Department of Psychology, University of Konstanz, Konstanz, Germany*

Abstract: For the study of functional organization and reorganization of the human cortex by means of electromagnetic source imaging, a measure of the location and spatial extent of neural sources is of interest. This study evaluates the cortical patch method (CPM), an iterative procedure introduced by Lütkenhöner et al. [1995] that models EEG / MEG activity by means of extended cortical patches. Anatomical information is used to constrain estimates of location and extent of neural sources that generate the measured evoked potential. Whereas minimum norm approaches use mathematical constraints to solve the ambiguity of the inverse problem, the CPM introduces constraints based on anatomical and physiological knowledge about neural mass activity. In order to test the proposed method, the simulated activity in an artificial sulcus was subjected to the CPM. The results show that even activity on opposing walls of a sulcus can be well reconstructed. The simulations demonstrate the usefulness and limits of the CPM in estimating the spatial extent of neural sources in the cerebral cortex. As an example, an application of the method on experimental somatosensory evoked potentials is presented in the Appendix. *Hum Brain Mapping 8:182–193, 1999.* © 1999 Wiley-Liss, Inc.

Key words: evoked potentials; source modeling; brain mapping; phantom limb pain; neuroplasticity; cortical reorganization

INTRODUCTION

Any external event activates a network of interconnected neurons in different brain structures. Early in the information-processing stream, activation patterns that overlap in time are often restricted to a few circumscribed brain areas. The electromagnetic activity generated by these neural sources generally can be described by electrical current dipole models (ECD) [Scherg and Von Cramon, 1986; Mosher et al., 1992; Elbert et al., 1995a; Lütkenhöner, 1998]. Using these models, information on the location, geometrical properties, and activity of the neural sources can be assessed. In the case of a focal activation that does not overlap with other activities in time, a single ECD model is appropriate. Multiple ECDs that model simultaneously active source configurations are useful if the spatio-temporal separation between the single sources is sufficiently large, i.e., if the separation exceeds a few centimeters [Lütkenhöner, 1996]. Thus multiple dipole

Contract grant sponsor: Deutsche Forschungsgemeinschaft (to C.B. and T.E.).

*Correspondence to: Christoph Braun, Eberhard-Karls-Universität, Institut für Medizinische Psychologie und Verhaltensneurobiologie, MEG-Zentrum, Otfried Müller Str. 47, D-72076 Tübingen, Germany. christoph.braun@uni-tuebingen.de

Received for publication 3 December 1998; accepted 7 May 1999.

models are adequate when there is one active focus per hemisphere or when there are time segments with little overlap between patches of activation. Both the single dipole and the multiple dipole approaches assume that the spatial extension across the active structure is smaller than the distance from the source to the sensor. This assumption is valid given that brain activity is often local for the components evoked early in the stream of brain responses.

For neocortical sources, problems with the ECD model may arise for several reasons. First, active cortical tissue may be relatively close to the sensors and, therefore, the assumption of a focal source might not be adequate. Second, the cortex is organized as a functionally distributed hierarchical system whereby sensory information is processed in multiple sensory representations that may be activated concurrently [e.g., Felleman and van Essen, 1991]. The re-entry principle may temporally bind multiple regions, leading to synchronous activation. Therefore, it is of interest not only where the center of a certain activation may be located, but also how large the extension of this activation may be.

For instance, in studies investigating the functional organization and reorganization of cortical representational zones, a measure of the spatial extent of sources would promise essential progress for the understanding of the consequences of cortical reorganization in humans. Effects of cortical reorganization following somatosensory deafferentation have been demonstrated by magnetic and electric source imaging by quantifying the shifts in the somatosensory representation [Elbert et al., 1994; Flor et al., 1995; Birbaumer et al., 1997]. Whereas these results in humans demonstrate macroscopic alteration based on ECD parameters, no direct evidence for the spatial extent of neural sources has been available in studies with humans. Using ECDs, spatial extent, or shrinkage in the representational zone is indicated at best indirectly by alterations of the dipole moment [Elbert et al., 1995b], by changes of the dipole location [Flor et al., 1995, 1997], and by changes in the residual variance. In such cases it is highly desirable to estimate the size of an activated brain area by directly modeling the source extension.

The cortical patch method (CPM) is one approach to determine changes in the size of neural sources using anatomical and physiological information. The first step of the algorithm involves dividing the cortical surface into small patches. Then the polarization of each patch is described by an associated current dipole. The orientation of this current flow is determined, in principle, by the orientation of the cortical patch, a measure that can be derived from MRI sections [Lütkenhöner et al., 1995; Lütkenhöner and Steinsträter, 1998]. From the measured EEG/MEG distribution on the scalp, the moment of these current dipoles can be estimated so that the corresponding electric potential/magnetic field fits the measured data. Using the cortical surface as an anatomical constraint, requesting the cortical patch to be contiguous and the dipoles perpendicular to the cortical surface, and using the activity distribution as a physiological constraint determine a possible solution of the inverse problem that otherwise has an infinite number of solutions.

Other strategies that model extended cortical sources exist besides the cortical patch model. Using the so-called minimum norm approaches, activity also can be restricted to cortical polarization. The algorithm estimates the moment of the individual dipoles such that both the sum of their norm and the fit error is minimal, resulting in an equation system that describes the dependency between the measured potential, the leadfield, and the current density. The various minimum norm models differ from each other by the definition of the norm or by the regularization of the equation system [Wischmann et al., 1992; Dale and Sereno, 1993; Wang, 1993; Pascual-Marqui et al., 1994]. The use of minimum norm constraints is attractive, not only because of the computational simplicity but also because the strategy reflects the principle of parsimony as the quadratic sum of the dipole activity is proportional to the energy of the source. It is, however, questionable whether such a rule reflects adequately the dynamics of cortical activity. In this study, we perform several simulations in order to validate the cortical patch approach. Additionally, the method was applied to experimental EEG data, presented in the Appendix.

The precision with which the source extension can be determined is limited by the error of measurement in the data that then enters the source analysis. Errors are mainly introduced through coherent EEG background activity and by imprecision of electrode placement. Furthermore, inaccuracies of the head model used to estimate the dipole parameters can seriously affect the outcome of the modeling procedure. In order to assess the limitations of the CPM, the impact of these error sources on the results for the source extension were also considered in this work. Simulations using different levels of noise led us to conclude that the CPM can assist in specifying minimal and maximal source extensions that are associated with measured EEG- or MEG-activity.

MATERIALS AND METHODS

Cortical patch model

The CPM represents a framework for modeling extended sources by combining data from EEG recordings, cortical surface reconstruction based on MRI scans, and prior information about the activity distribution of the fitted sources. It requires: (1) triangulation of the cortical surface, (2) a head model that describes the electrical and geometrical properties of the head and its tissues, and (3) a fit procedure that searches for regions of cortical polarization that best produces the measured electrical activity at the scalp.

Anatomical and physiological constraints

The reconstruction of the cortical surface on the basis of MRI scans was performed with the CURRY software [Fuchs et al., 1994]. By specifying an appropriate level of brightness, the cortical surface including gyri and sulci can be extracted from MR brain images resulting in a list of surface triangle coordinates. The active triangles are postulated to cover a contiguous surface because the active cortical area is assumed to be a nondisjunctive area. If the neural substrate within a triangle is active, the triangle becomes polarized. The cause of this polarization is a current flow generated by the pyramidal cells of the cortex [Birbaumer et al., 1990]. This activity can be described by a current dipole with an orientation parallel to the current flow and placed in the center of gravity of the active triangle.

Because very little is currently known about the profile of the current source density across an active cortical patch, a constant polarization is assumed, i.e., all active elements have the same constant current source density. Consequently, the moment of a single dipole is proportional to the area of the associated triangle. Primarily, the CPM is intended to estimate the extent of one source, but it can be extended to several sources by using multiple patches that grow simultaneously. Whether or not one or more sources are active can be determined by principal component analysis, the MUSIC approach [Mosher et al., 1992], or by multiple equivalent dipole models and has to be specified within the cortical patch algorithm. Additionally, if there is knowledge about the origin of the neural source under study, it is possible to include this information by reducing the triangulated cortical surface to the relevant brain region, thereby reducing the manifold of possible solutions and excluding those that do not make sense from a morphological or functional point of view.

In studies investigating the reorganization of primary sensory cortices, changes of the source extent are relevant. In the present work, we focus on the characteristics of the central sulcus for both the simulations and the experimental results (see Appendix).

TABLE I. Electrical conductivities and eccentricities of the four layers of the spherical head model*

Layer	Anatomical structure	Eccentricity	Conductivity $[1/\Omega \cdot m]$
1	Brain tissue	0.8977	$330.0 \cdot 10^{-3}$
2	Cerebro-spinal fluid	0.9205	$1000.0 \cdot 10^{-3}$
3	Skull	0.9659	$4.2 \cdot 10^{-3}$
4	Scalp	1.0000	$330.0 \cdot 10^{-3}$

* Geddes and Baker, 1967.

Physical basis

The potential distribution of all the dipoles on the scalp was calculated using a spherical head model with four concentric layers of different electrical conductivity representing brain tissue, cerebro-spinal fluid, skull, and scalp (Table I) [Geddes and Baker, 1967; Cuffin and Cohen, 1979]. The potential of the dipoles associated with the n triangles at m electrodes can be written as a vector $U^T = (U_1, \ldots, U_m)$. Letting $C(m,n)$ be the leadfield matrix, which describes the relationship between the parameters of a dipole with moment 1 and the corresponding potential at a single electrode, $S^T = (S_1, \ldots, S_n)$ be a vector containing the area of the n triangles, ρ be the current source density and $\delta(n,n)$ be a diagonal matrix with zeros as off-diagonal elements and diagonal elements either 1 or 0 depending on whether the respective triangle is turned on or off [Srebro, 1994], then

$$U = \rho \cdot C \cdot \delta \cdot S \tag{1}$$

The measured potential being $\tilde{U}$, the residual variance is defined by

$$r = (\tilde{U} - U)^T \cdot (\tilde{U} - U) / \tilde{U}^T \cdot \tilde{U} \tag{2}$$

If a certain pattern of active triangles is specified by matrix δ, then the current source density of the active triangles leading to the best fit can be calculated by linear regression:

$$\rho = (S^T \cdot \delta \cdot C^T \cdot C \cdot \delta \cdot S)^{-1} \cdot (C \cdot \delta \cdot S)^T \cdot \tilde{U}. \tag{3}$$

Fit procedure

The basic principle of the CPM comprises the modeling of the scalp potential by adding single surface elements (patches) to a contiguous active cortical patch so that its produced electrical potential distribution reproduces the measured topography. The method is an iterative approach, involving the steps below.

1. Searching for a starting triangle (first seed patch) whose activity produces the best fit of the measured potential. This is achieved by the minimization of the residual variance, i.e., by minimizing the difference between the modeled and the measured data.
2. Determining triangles adjacent to the starting patch.
3. Searching for a combination of neighboring triangles that, when combined with the seed patch, results in a lowered residual variance.
4. Updating the seed patch by adding the triangles from the former step.
5. Replicating steps 1–4 until a global minimum of the residual variance is reached.

These steps are described in detail below.

1. Seedpoint (first seed patch). To determine the seedpatch, we assume that from the total number of triangles representing the extracted surface, the triangle that best fits the measured potential belongs to the active source. By switching on only one triangle, i.e., one diagonal element of δ, the current source density in Equation (3) can be determined by linear regression, and the corresponding residual variance can be calculated (Equations (1) and (2)). The triangle with the lowest residual variance is chosen as first seed patch in the further steps of the analysis.

2–4. Growth of the source. The cortical patch model is designed to find a contiguous active cortical area. This condition can be achieved by allowing only those triangles adjacent to the seed patch to be active within one growth step. The neighborhood between two triangles is defined as having one side in common. Using the leadfield matrix C, one can calculate at the electrodes the electric field distribution, which is produced by the seed patch together with every combination of its neighboring triangles. Within one step of iteration, at least one triangle is regarded to be active. There are $2^N - 1$ possible combinations of N neighboring triangles and the seed patch that correspond to $2^N - 1$ possible electrical field distributions.

The residual variance for each patch combination is calculated, and the variance with the smallest value is chosen to form the seed patch for the next iterative step. To obtain a contiguous active area, inactive triangles that are totally surrounded by active ones are added to the seedpatch.

5. Termination of growth. The replication of the steps 1–4 leads to a growth of the source. The steps of source growth are replicated until the global minimum of the residual variance is passed.

Simulated data

In order to test the CPM, an artificial sulcus consisting of 1,200 triangles was defined (Fig. 1). As an example, the shape and orientation of the artificial sulcus were designed to resemble the somatosensory cortex, for which an experimental study is presented in the Appendix. The outer radius of the sulcus was 80 mm, the inner radius 70 mm. The extended source consisted of 150 contiguous triangles that were located mainly on one wall of the sulcus. Of the active triangles, 20% were located on the opposing wall. Each triangle was associated with a dipole whose orientation was orthogonal to the corresponding triangle and whose moment was proportional to the triangle area. The potential distribution of this active cortical patch was calculated at 60 electrodes using the same four-layer spherical head model as for the source estimation. Electrodes covered most of the scalp area over the sulcus. This particular geometry of the source was used to investigate whether the CPM is able to identify sources spread out on both sides of a sulcus, because in this case the activities on the opposing walls tend to cancel each other. A similar activation pattern has been used as test condition for other approaches [Okada, 1985; Nunez, 1986; Wang, 1994].

Influence of activity distribution

In order to investigate the error that is introduced by assuming a constant activation density across the active cortical surface, the effect of two different activity distributions of an artificial source were analyzed. The source consisted of 44 triangles, which formed three concentric regions (Fig. 1) and had a total extension of 65.3 mm^2. The first case dealt with a uniform activity distribution where the activity of all three regions was defined proportional to their surface. In the second case, the activity of the innermost region was defined four times proportional to its surface, the

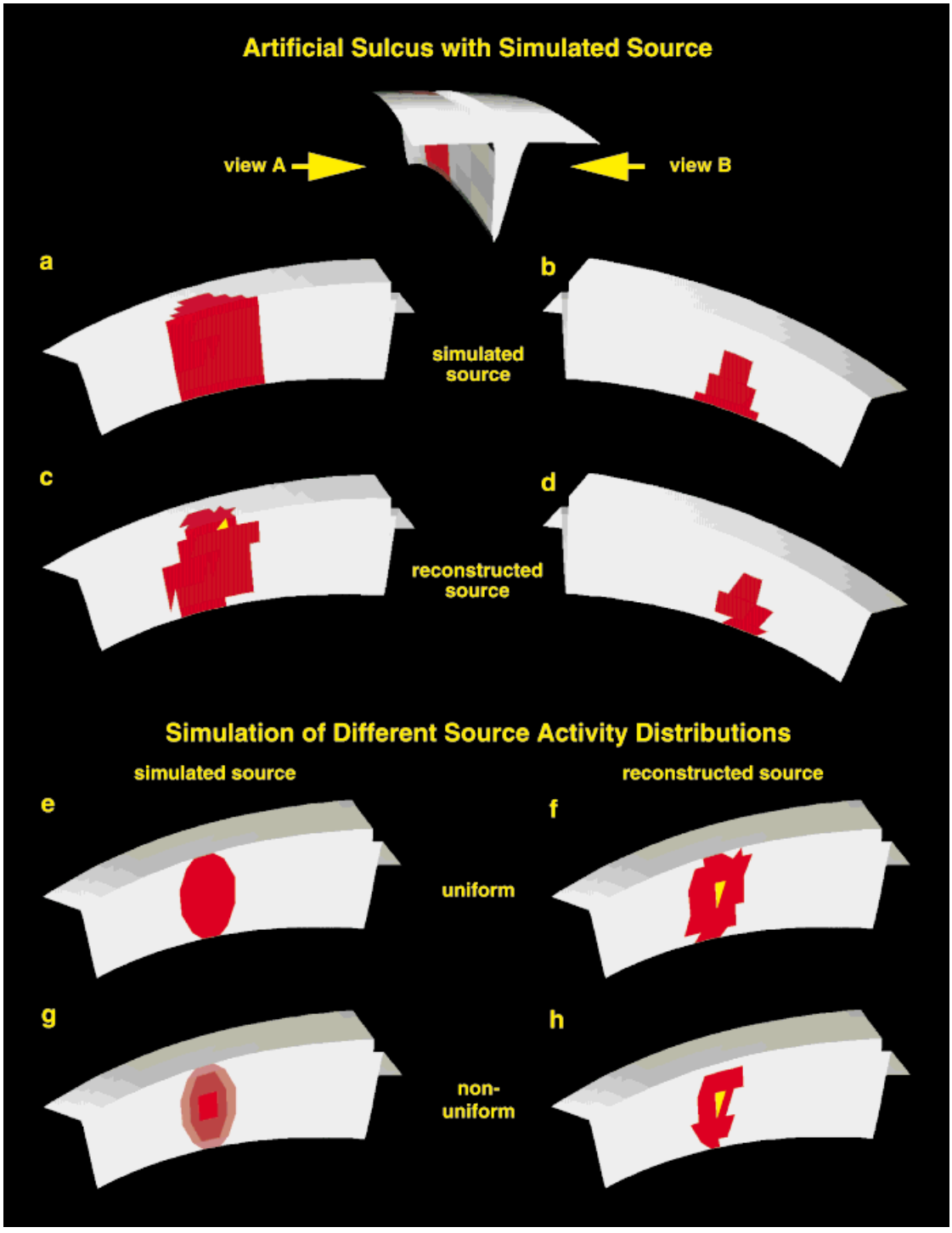

Fig. 1.

Artificial sulcus with simulated sources. (a–d) To develop and validate the cortical patch method, an artificial sulcus and an artificial source located on both walls of the sulcus were generated. (**a,b**) The sulcus consisted of 1,200 triangles with an average extension of 1.1 mm^2 and the source was made of 150 triangles and had a total extent of 183.8 mm^2. The potential of the artificial source was calculated and subjected to the cortical patch method. (**c,d**) The solution provided by the cortical patch method consisted of 120 triangles located on both sides of the sulcus and had a total extent of 162.1 mm^2. The seed triangle is colored yellow. (e–h) In order to investigate the error that is introduced by assuming a constant activation density across the active cortical surface, the effect of two different activity distributions of an artificial source were analyzed. The source consisted of 44 triangles that formed three concentric regions and had an total extension of 65.3 mm^2. To visualize the different source activity distributions, different shades of red were used. Seed triangles are colored yellow. (**e**) The first case dealt with a uniform activity distribution where the activity of all three regions was defined proportional to their surface. (**g**) In the second case, the activity of the innermost region was defined four times proportional to its surface, the middle region two times proportional to its surface, and the outer region directly proportional to its surface. (**f**) The solution source for the uniform distribution had an extension of 70.2 mm^2. (**h**) In the case of the nonuniform activity distribution, the solution source had an extension of 44.3 mm^2.

middle region two times proportional to its surface, and the outer region directly proportional to its surface.

Influence of uncorrelated and correlated noise

In general, recorded EEG data are contaminated with noise, which leads to deterioration of the accuracy of the source reconstruction [Braun et al., 1997]. To assess the impact of noise on the size of the estimated active brain area, three different levels (1%, 2%, and 5%) of uncorrelated and correlated noise were included in the simulation. Uncorrelated noise was simulated by adding random numbers with a mean of 0 to all 60 electrodes. The correlated noise was modeled by averaging the potential distribution of 1,000 arbitrarily placed dipoles at an eccentricity of 70 mm. The standard deviation of the uncorrelated and correlated noise was selected such that the ratio of the root mean square of noise and signal resulted in the specified value of the signal-to-noise ratio. In order to obtain reliable information about the impact of noise on the extended source modeling algorithm, we created 10 different data sets for each noise level and subjected them to the CPM.

Influence of electrode positioning error

To investigate the influence of erroneous electrode localization on the CPM, we investigated two error levels of electrode position data. The 60 electrode positions were randomly misplaced such that the standard deviation of the misplaced distance was 5 mm and 10 mm. Each of these positioning error levels was simulated 10 times.

Influence of head model errors

In the fit procedure, we compared the measured potential distribution with the field generated by the forward calculation for the active source. This forward solution was calculated for a spherical head model with four concentric layers, characterized by the parameters specified in Table I. As the erroneous specification of head model parameters is supposed to influence the outcome of the CPM, it is of interest to investigate the relationship between variations of these parameters and their effect on the source extension. We focused our analysis on the skull thickness because, of the four layers, the skull has the smallest electrical conductivity and is mainly responsible for the smearing of the scalp potentials [Gevins et al., 1991]. We calculated the forward solution for a skull thickness of 9.8 mm and 12.3 mm. We then applied both data sets to the CPM where we used the default value for the skull thickness of 7.3 mm, which, as seen in Table I, corresponds to an outer radius of the spherical head model of 92.0 mm.

RESULTS

When the residual variance as a function of source extension is compared among all different simulations, a typical shape can be identified: a steep decline of the residual variance at the beginning, then a broad flat region followed by a smooth increase. The magnitude of the residual variance in the flat region and the width of that region were found to depend on the level of noise. For all simulated sources of noise, i.e., uncorrelated and correlated measurement noise, electrode positioning errors and inaccuracies of the head model parameters, it was found that the higher the noise level, the flatter the residual variance function. An example is illustrated in Figure 2, where the residual variance is plotted for different levels of uncorrelated simulated EEG noise.

The 10 simulations performed for each EEG noise level led to a residual variance minimum whose range depended on whether the noise was correlated or not. In the case of uncorrelated noise, these ranges were clearly separated between the investigated noise levels, whereas for correlated noise they overlapped remarkably (Table II). The simulations performed for both electrode position error levels led to slopes that were strongly overlapping. In the case of the head model error, the larger the error in specification of the skull thickness parameter, the flatter the slope of the residual variance.

The shape of the residual variance function indicates that all sources in the flat region of the residual variance function fit the measured potential comparably well, but differ considerably in their extension. Therefore, it is only meaningful to specify the minimum and maximum extension of a source that fits the measured data with a given residual variance if noise is present.

Application of the CPM to the potentials of the simulated source located at the two walls of an artificial sulcus resulted in a source consisting of 120 triangles. Of these, 109 active triangles belonged to the initial 150. The total size of the reconstructed area (162.1 mm^2) was somewhat smaller than the simulated area (183.8 mm^2) (Fig. 1). As can be seen from Figure 1, the activity extension onto the other wall of the sulcus could be reproduced by the method. The shape of the reconstructed dipolar extended source differed only slightly from the original source.

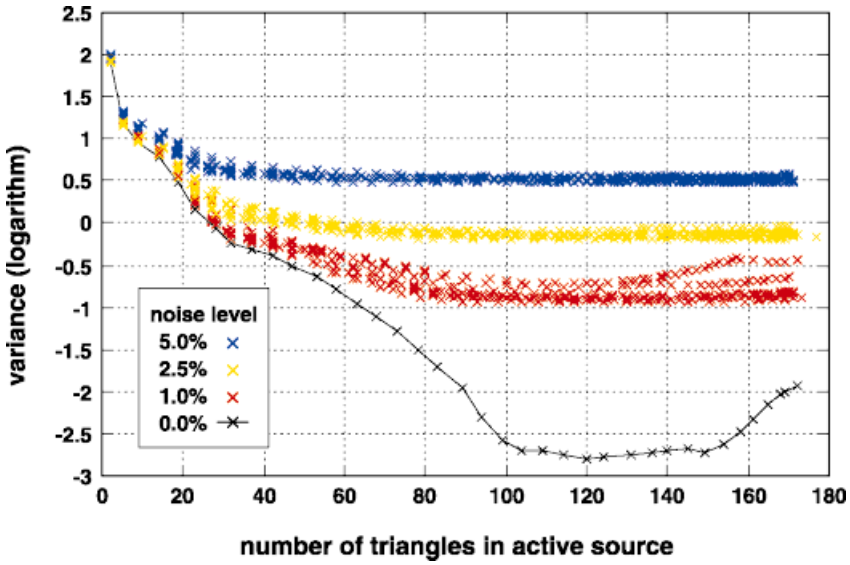

Fig. 2.
Impact of uncorrelated noise. Dependency of the residual variance (logarithmic values) from the source extension, represented by the number of triangles, is plotted for four different signal-to-noise ratios: 0.0%, 1.0%, 2.5%, and 5.0%. For each noise level (except 0.0%), 10 simulations were performed to obtain reliable information.

The analysis of the two simulated sources with the same extension but different source activity distributions showed that in the case of the nonuniform activity distribution, the solution source had a smaller extension (44.3 mm^2) than the default one (65.3 mm^2). The solution source for the uniform distribution had an extension of 70.2 mm^2, which is similar to the default value (Fig. 1).

TABLE II. Ranges of the minimum of residual variance function and corresponding number of triangles in the four different error types and levels*

Error		Range of minimum residual variance (log)			Range of triangle number in source		
Type	Level	Min	Max	Mean	Min	Max	Mean
Zero noise	0.0	−2.793	−2.793	−2.793	120	120	120
Uncorrelated noise	1.0	−0.995	−0.759	−0.913	114	139	126
%	2.5	−0.087	−0.191	−0.145	103	159	132
(signal-to-noise ratio)	5.0	0.425	0.500	0.464	84	160	126
Correlated noise	1.0	−0.986	0.090	−0.337	102	157	126
%	2.5	−0.502	0.883	0.420	94	172	121
(signal-to-noise ratio)	5.0	0.035	1.487	1.015	61	172	117
Electrode position	5.0	0.544	1.222	0.861	30	174	140
(mm standard deviation)	10.0	1.152	1.954	1.480	15	174	72
Skull thickness (mm)	9.8	−0.761	−0.761	−0.761	149	149	149
(default: 7.3 mm)	12.3	−0.329	−0.329	−0.329	173	173	173

* For uncorrelated noise, correlated noise, and electrode position error, the values in column 3 and 4 represent the lowest (Min), respectively, highest value (Max) of the residual variance for 10 performed simulations. For the same error types, columns 6 and 7 represent the lowest (Min) and highest number (Max) of source triangles corresponding to the minimum of the residual variance for the simulations. For the skull thickness, two different values were analyzed.

DISCUSSION

The aim of this study was to validate an extended source modeling approach, the cortical patch model. The simulations performed showed that it is possible to localize extended sources and to quantify the size of the active brain area from simulated EEG data. Even in the rather difficult case of opposing activity on the anterior and posterior wall of an artificial sulcus, where both activities tend to cancel each other when viewed from distant electrodes, the algorithm enabled the identification of both activities. However, the simulations also revealed that the method is limited by the different sources of noise and errors that are associated with the measurement and analysis of evoked potentials.

Impact of noise and errors on the source extension

Environmental noise, background brain activity, inaccuracies in measuring the electrode positions, and errors in specifying the appropriate head model flatten the slope of the residual variance function (the relationship between source extension and unexplained variance). Beyond the bend where the slope becomes flat, there are many source extensions that fit the potential data comparably well, making it impossible to specify the absolute size of an activated cortical area. Furthermore, growing the source beyond the bend improves the residual variance so slightly that we conclude only noise is explained and no longer data. Consequently, for a specific noise level, a minimum source size can be specified that best explains the measured data. Simulations showed that higher noise levels move the minimum source extent toward lower values. This leads to an underestimation of the source extent, which is more predominant for higher noise levels. If the extension of activated cortical areas is compared between different experimental conditions, it is therefore essential that the noise levels are similar. Otherwise it is not possible to decide whether an effect is due to experimental manipulations or due to differences in the noise level.

One strategy to improve the accuracy of the CPM would be to reduce the impact of noise and error sources. Environmental noise and background activity cannot be influenced, but it is possible to diminish the errors of the head model and electrode positioning. All data presented here were calculated with a four-shell spherical head model. Due to the model's simplification of electrical properties of the head, errors in location and extension of the computed source patch may be introduced. These deviations between the spherical head model and the actual head properties may be greater than the amount of change in the residual variance, especially when triangles are added to a larger source. Using realistic head models might improve the estimation of the source extension by the cortical patch model. Work by Lütkenhöner et al. [1995], however, indicates that such an improvement may be small for generator structures in regions with homogenous electrical conductivities that fit well with the spherical model. This seems to be the case for the Brodman's area 3b, i.e., the somatosensory representation modeled in the example presented in the Appendix.

Spatial resolution of the extended source

The spatial resolution of the estimated source depends on the resolution of the reconstructed cortical surface, i.e., on the triangle size. The smaller the surface elements, the more accurate the cortical surface and the topology of the extended source. A high resolution means, however, that the source is composed of a large number of patches. Consequently, more steps are necessary to compute the source model. This, in turn, demands a much longer computation time because the number of possible triangle combinations grows exponentially. The results presented here were computed with triangles having an average area of 2.6 mm^2, corresponding to an average distance between the single support points of 2.5 mm. In the case of the artificial sulcus, 3 hours of CPU time on a HP B160L (160 MHz) workstation were required for 200 source triangles.

Comparison with other approaches

Besides the presented method, there are other algorithms available to model extended sources using anatomical constraints. Most of them are based on a minimum norm constraint, which minimizes the resulting activity of the modeled sources [Wang, 1993; Pascual-Marqui et al., 1994]. As no data exist proving that the brain realizes this principle; this assumption seems to be rather arbitrary. The assumption of a constant current source density across the whole source extension as it is used in the presented method is also only an approximation and probably problematic, too. But, in contrast to the minimum norm method, our extended source model principally supports the incorporation of detailed physiological knowledge about the source activity distribution. Additionally, the source fitted with the CPM is contiguous, which better fits the concept of functional units of the brain that are spatially organized. An analysis of the two different

source activity distributions revealed that for the nonuniform distribution, the solution source found by the CPM had a smaller extension than the default source. We have to assume that real cortical sources indeed have a nonuniform activity distribution. This means that source extensions calculated by the CPM tend to underestimate the true size of the source.

Simulations showed that the CPM is able to model sources spread out on opposing walls of a sulcus, which represents a rather difficult case for the inverse problem. Using a source pattern similar to the one used in our simulation, Wang [1994] demonstrated that the minimum norm method is able to model activities located on opposing walls of a sulcus, whereas other inverse methods have difficulties discriminating the individual sources [Okada, 1985; Nunez, 1986].

Although each method finds a unique solution of the ill-posed inverse problem by using additional constraints, the presence of noise introduces an additional unsolvable ambiguity. Therefore, the ambiguity that results from the flatness of the residual variance function in the cortical patch model is not only a problem of this method. In contrast, it is inherent to all extended source models because multiple solutions always exist that differ only slightly in their fit quality. In minimum norm approaches, a regularization of the equation system depending on the noise level has to be performed to yield meaningful results [Wischmann et al., 1992; Fuchs et al., 1994]. In contrast, the regularization determines the source extension. Consequently, in these methods higher noise levels result also in smaller source sizes. An additional approach that meets the requirements of the ambiguity of the inverse problem in that it examines various likely solutions in terms of their probability combines prior information with a Bayesian inference framework [Schmidt et al., 1998]. The multiplicity of solutions reflects the ambiguity of the inverse problem and yields to a probability distribution for the number, location, and extent of active sources. From this distribution, the most probable source is chosen. With increasing noise, the probability distribution of the individual parameters becomes similar to an even distribution. Therefore, the most probable solution cannot be definitely determined.

Extensions of the model

Even if the presented model deals with only one source, the method can be extended to several sources in principle. If each source is associated with a seed point, each source may grow around its starting point. As in multiple dipole models, however, interaction between the different sources may cause uncontrolled growing of the sources. Yet, the assumption of a constant activation density of all sources restrains the interaction between the different sources. Even in the case of opposing activity that has been simulated in the present study, no extensive growing has occurred, although part of the activation on both walls of the sulcus cancel each other.

Unlike in the presented simulations where the potential distribution for only one time point was analyzed, it is possible to include a larger time range for the fitting and to expand the model to a spatio-temporal approach. That means that several sources are assumed whose activity changes over time.

Conclusions

The simulations demonstrate that the presented cortical patch method is able to assess the size of an extended cortical source; therefore, the method can be viewed as an additional tool for the source analysis of evoked potentials. It has been shown that the method is limited by the different sources of noise and error that are associated with the measurement of evoked potentials. As a result, no absolute size of the source can be obtained. However, if the source extent of different experimental conditions is compared, the cortical patch method is a helpful tool, provided the noise level is similar for all conditions.

APPENDIX

In order to illustrate the CPM for an experimental data set, we studied the effects of cortical reorganization of the somatosensory representation of the lip induced by analgesia in a single subject with upper extremity amputation.

Dipole source analysis of somatosensory evoked potentials elicited by tactile stimulation of the lip have shown that patients with amputations who experience severe phantom pain are likely to exhibit massive cortical reorganization [Flor et al., 1995]. In upper arm amputees, the face area ‘‘invades’’ the cortical zone that had formerly represented the now absent hand and fingers. If the brachial plexus on the affected side is blocked by an anesthetic, a lateral shift of the cortical representation of the lip toward a normal localization can be observed, provided that the analgesia caused a relieve from phantom pain [Birbaumer et al., 1997]. As the experimental design and the results have been published in Birbaumer et al. [1997], method and procedure are presented only in brief.

Method

Evoked potentials elicited by stimulation of the right and left lower lip were measured two times: once before blockade of the right brachial plexus with the anesthetic mepivacaine combined with suprarenin and once during anesthesia. Each time, 1,000 trials of evoked responses were recorded at 60 electrodes that were affixed to an elastic cap in a 6 × 10 rectangular array centered over Cz and spaced 3 cm apart. A linked ear reference was used. The sampling rate was set to 1,000 Hz; the frequencies of the lowpass and the highpass filter were 200 and 0.1 Hz, respectively. It is known that SI (areas 3b and 1) is the first cortical area that becomes activated, whereas SII and posterior parietal cortex show EEG/MEG-responses only at a somewhat later interval (beyond 80–90 ms), [Hari et al., 1993; Elbert et al., 1995a]. As we model here components in the 35–60 ms latency range, it is known a priori that activities result from SI. Whereas in principle it is possible to allow sources anywhere on the whole cortical sheet, additional constraints should be introduced whenever available. Therefore, a region 2 cm anterior and posterior to the central sulcus of both hemispheres was used as the region of interest for the source reconstruction of the evoked potentials (Fig. 3, top).

Results

The signal-to-noise ratio of the experimental data, measured as root-mean-square (RMS) ratio between amplitudes of the evoked response and the prestimulus baseline, was 3.04 for the condition ''before anesthesia'' and 5.25 for the ''during anesthesia'' condition for right lower lip stimuli and 5.14 and 5.55, respectively, for left lower lip stimuli. When extended sources were modeled, the slope of the residual variance for the right lower lip differed for both conditions (note that the right hand and arm were amputated): first, the magnitude of the residual variance of the extended source fit was lower for the ''before anesthesia'' condition than for the ''during anesthesia'' condition; second, both the local and the global minimum was reached for different numbers of triangles. At the beginning of the iteration, a steep decline of the residual variance into a local minimum was identified: 12 triangles (23.9 mm^2) for the ''before anesthesia'' condition and seven triangles (14.9 mm^2) for the ''during anesthesia'' condition. In contrast to the results for the right lower lip, the slope of the residual variance for the left lower lip revealed only slight differences between the ''before anesthesia'' and the ''during anesthesia'' conditions. The residual variance was of the same order of magnitude and the number of triangles in the source was identical: three triangles (12.8 mm^2) for the ''before anesthesia'' condition and three triangles (11.1 mm^2) for the ''during anesthesia'' condition. These results suggest that the extension of the cortical representation of the lower lip contralateral to the amputation decreases during anesthesia (Fig. 3), whereas no change in size of the representation area can be found on the intact side of the body (Fig. 3).

Discussion

In patients with upper extremity amputation, the deafferentation of peripheral input from the stump causes functional reorganization of the primary somatosensory cortex [Pons et al., 1991; Pascual-Leone and Torres, 1993; Elbert et al., 1994; Flor et al., 1995]. Birbaumer et al. [1997] demonstrated that during the blockade of the brachial plexus with local anesthesia, the cortical representation of the lip that had moved toward the brain region of the now amputated hand returns toward the region that supposedly represented the lip prior to amputation. This region is assumed to be located at the mirror image position of the lip representation of the intact body side. It is also assumed that this shift in localization is accompanied by a reduction in the size of the representational zone of the lip. Such changes should not occur for the cortical representations of the intact side of the body. With the CPM, we could provide evidence in support of this hypothesis.

The application of the CPM on experimental data demonstrated that in principle it is possible to verify changes in the extent of the cortical representation caused by reorganization. As has been pointed out for the simulation results, the signal-to-noise ratio of the measured potentials is of great importance. Although it seems that even in low noise measurements, the minimum of the residual variance function is too flat to get a precise estimate of the absolute source extension, conclusions about changes of the size of a cortical source can be drawn reliably if two experimental conditions are compared.

ACKNOWLEDGMENTS

We thank Dr. Pedro Montoya for making the experimental data available to us.

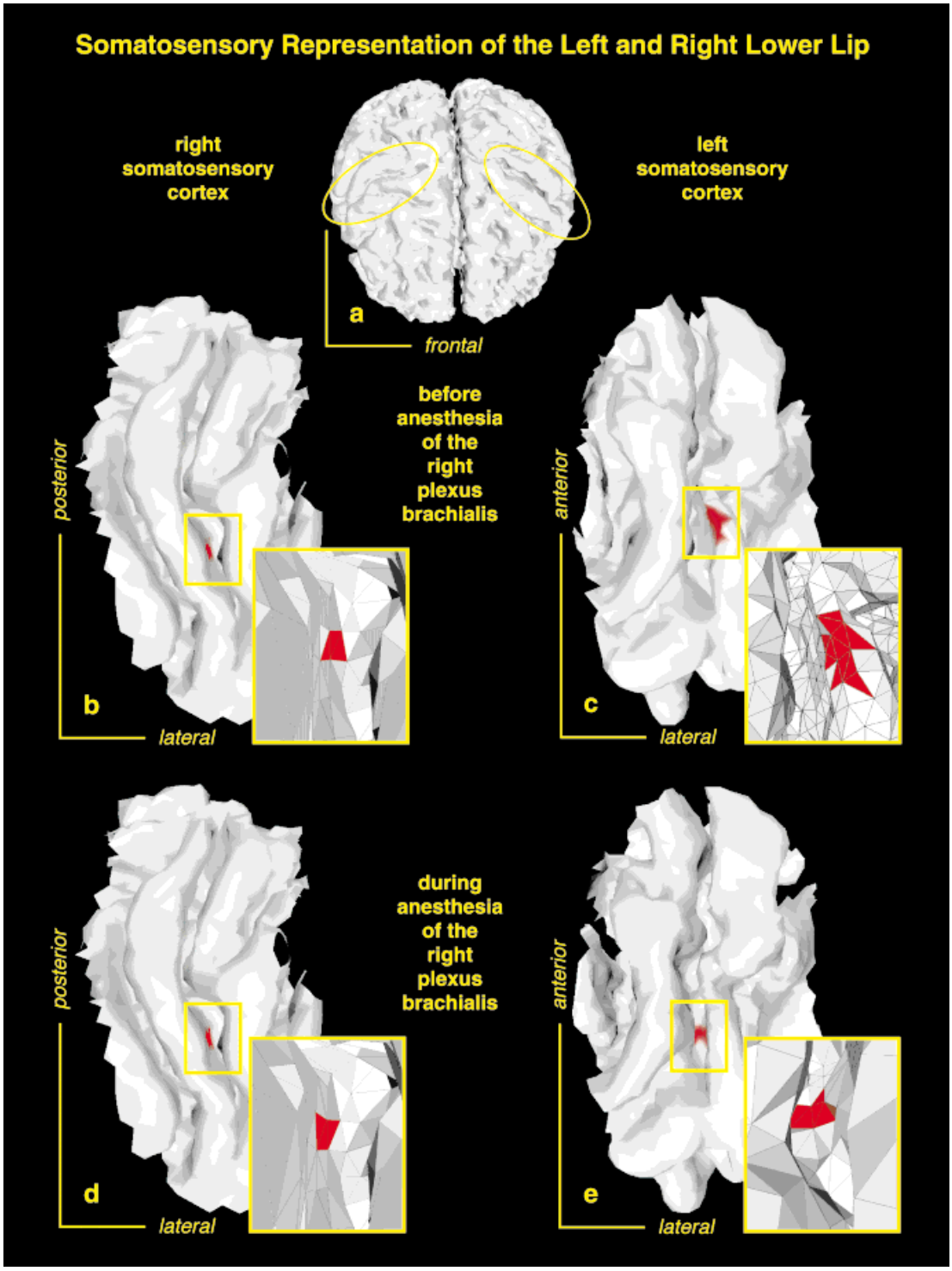

Fig. 3.

Somatosensory representation of the right and left lower lip before and during the anesthesia of the right plexus brachialis for a subject with amputated right arm. (**a**) To decrease computation time, an area situated 2 cm around the sulcus centralis in both hemispheres was used in determining the source of the SEPs of the right and left lower lip elicited under two conditions: before anesthesia and during anesthesia of the right plexus brachialis. (**b,c**) For the SEPs of the left and right lower lip in the ''before anesthesia'' condition, the cortical patch method revealed a source consisting of three triangles (12.8 mm^2) for the left lower lip and 12 triangles (23.9 mm^2) for the right lower lip. (**d,e**) For the SEPs of the left and right lower lip in the ''during anesthesia'' condition, the cortical patch method revealed a source consisting of three triangles (11.1 mm^2) for the left lower lip and seven triangles (14.9 mm^2) for the right lower lip.

REFERENCES

Birbaumer N, Elbert T, Canavan AG, Rockstroh B. 1990. Slow potentials of the cerebral cortex and behavior. Physiol Rev 79:1–41.

Birbaumer N, Lutzenberger W, Montoya P, Larbig W, Unertl K, Töpfner S, Grodd W, Taub E, Flor H. 1997. Effects of regional anesthesia on phantom limb pain are mirrored in changes in cortical reorganization. J Neurosci 17:5503–5508.

Braun C, Kaiser S, Kincses WE, Elbert T. 1997. Confidence interval of single dipole locations based on EEG data. Brain Topogr 10:31–39.

Cuffin BN, Cohen D. 1979. Comparison of the magnetoencephalogram and electroencephalogram. Electroenceph Clin Neurophysiol 47:132–146.

Dale AM, Sereno MI. 1993. Improved localization of cortical activity by combining EEG and MEG with MRI cortical surface reconstruction: A linear approach. J Cognitive Neurosci 5:162–176.

Elbert T, Flor H, Birbaumer N, Knecht S, Hampson S, Larbig W, Taub E. 1994. Extensive reorganization of the somatosensory cortex in adult humans after nervous system injury. Neuroreport 5:2593–2597.

Elbert T, Junghofer M, Scholz B, Schneider S. 1995a. The separation of overlapping neuromagnetic sources in first and second somatosensory cortices. Brain Topogr 7:275–282.

Elbert T, Pantev C, Wienbruch C, Rockstroh B, Taub E. 1995b. Increase of cortical representation of the fingers of the left hand in string players. Science 270:305–307.

Felleman DJ, van Essen DC. 1991. Distributed hierarchical processing in the primate cerebral cortex. Cerebral Cortex 1:1–47.

Flor H, Elbert T, Knecht S, Wienbruch C, Pantev C, Birbaumer N, Larbig W, Taub E. 1995. Phantom-limb pain as a perceptual correlate of cortical reorganization following arm amputation. Nature 375:482–484.

Flor H, Braun C, Elbert T, Birbaumer N. 1997. Extensive reorganization of primary somatosensory cortex in chronic pain patients. Neurosci Lett 224:5–8.

Fuchs M, Wagner M, Wischmann HA, Ottenberg K, Dössel O. 1994. Possibilities of functional brain imaging using a combination of MEG and MRT. In: Pantev C, Elbert T, Lütkenhöner B (eds): Oscillatory Event Related Brain Dynamics. New York: Plenum Press, pp 435–457.

Geddes LA, Baker LE. 1967. The specific resistance of biological materials: A compendium of data for the biomedical engineer and physiologist. Med Biol Eng 5:271–293.

Gevins A, Le J, Brickett P, Reutter B, Desmond J. 1991. Seeing through the skull: advanced EEGs use MRIs to accurately measure cortical activity from the scalp. Brain Topogr 4:125–131.

Hari R, Karhu J, Hämäläinen M, Knuutila J, Salonen O, Sams M, Vikman V. 1993. Functional organization of the human first and second somatosensory cortices: A neuromagnetic study. Eur J Neurosci 5:724–734.

Lütkenhöner B, Menninghaus E, Steinsträter O, Wienbruch C, Gissler HM, Elbert T. 1995. Neuromagnetic source analysis using magnetic resonance images for the construction of source and volume conductor model. Brain Topogr 7:291–299.

Lütkenhöner B. 1996. Current dipole localization with an ideal magnetometer system. IEEE Trans Biomed Eng 43:1049–1061.

Lütkenhöner B. 1998. Dipole localization accuracy as a function of the area covered by the magnetometer system. In: Aine CJ, Flynn ER, Okada Y, Stroink G, Swithenby SJ, Wood CC (eds): Biomag96: Advances in Biomagnetism Research. New York: Springer-Verlag (in press).

Lütkenhöner B, Steinsträter O. 1998. High-precision neuromagnetic study of the functional organization of the human auditory cortex. Audiol Neurootol 3:191–213.

Mosher JC, Lewis PS, Leahy RM. 1992. Multiple dipole modeling and localization from spatio-temporal MEG data. IEEE Trans Biomed Eng 39:541–557.

Nunez PL. 1986. The brain's magnetic field: Some effects of multiple sources on localization methods. Electroenceph Clin Neurophysiol 63:75–82.

Okada Y. 1985. Discrimination of localized and distributed current dipole sources and localized single and multiple sources. In: Weinberg H, Stroink G, Katila T (eds): Biomagnetism, Application and Theory. New York: Pergamon Press, pp 266–272.

Pascual-Leon A, Torres F. 1993. Plasticity of the sensorimotor cortex representation of the reading finger in Braille readers. Brain 116:39–52.

Pascual-Marqui RD, Michel CM, Lehmann D. 1994. Low resolution electromagnetic tomography: A new method for localizing electrical activity in the brain. Int J Psychophysiol 18:49–65.

Pons TP, Garraghty AK, Ommaya AK, Kaas JH, Taub E, Mishkin M. 1991. Massive cortical reorganization after sensory deafferentation in adult macaques. Science 252:1857–1860.

Scherg M, Von Cramon D. 1986. Evoked dipole source potentials of the human auditory cortex. Electroencephalogr Clin Neurophysiol 65:344–360.

Schmidt DM, George JS, Wood CC. 1998. Bayesian inference for neural electromagnetic source localization. NeuroImage 7:665.

Srebro R. 1994. Continuous current source inversion of evoked potential fields in a spherical model head. IEEE Trans Biomed Eng 41:997–1003.

Wang JZ. 1993. Minimum-norm least-squares estimation: Magnetic source images for a spherical model head. IEEE Trans Biomed Eng 40:387–396.

Wang JZ. 1994. MNLS inverse discriminates between neuronal activity on opposite walls of a simulated sulcus of the brain. IEEE Trans Biomed Eng 41:470–479.

Wischmann HA, Fuchs M, Dossel O. 1992. Effect of the signal-to-noise ratio on the quality of linear estimation reconstructions of distributed current sources. Brain Topogr 5:189–194.